Fabrication and optical characterization of microstructures in poly(methylmethacrylate) and poly(dimethylsiloxane) using femtosecond pulses for photonic and microfluidic applications

Deepak L. N. Kallepalli,[1] Narayana Rao Desai,[1,3] and Venugopal Rao Soma[2,*]

[1]School of Physics, University of Hyderabad, Hyderabad 500046, India

[2]Advanced Centre of Research in High Energy Materials, University of Hyderabad, Hyderabad 500046, India

[3](dnrsp@uohyd.ernet.in)

*Corresponding author: svrsp@uohyd.ernet.in

Received 10 February 2010; revised 28 March 2010; accepted 29 March 2010;
posted 31 March 2010 (Doc. ID 123868); published 23 April 2010

We fabricated several microstructures, such as buried gratings, surface gratings, surface microcraters, and microchannels, in bulk poly(methylmethacrylate) (PMMA) and poly(dimethylsiloxane) (PDMS) using the femtosecond (fs) direct writing technique. A methodical study of the diffraction efficiency (DE) of the achieved gratings was performed as a function of scanning speed, energy, and focal spot size in both PMMA and PDMS. An optimized set of writing parameters has been identified for achieving efficient gratings in both cases. The highest DE recorded in a PDMS grating was ~10% and ~34% in a PMMA grating obtained with an 0.65 NA (40X) objective with a single scan. Spectroscopic techniques, including Raman, UV-visible, electron spin resonance (ESR), and physical techniques, such as laser confocal and scanning electron microscopy (SEM), were employed to examine the fs laser-modified regions in an attempt to understand the mechanism responsible for physical changes at the focal volume. Raman spectra collected from the modified regions of PMMA indicated bond softening or stress-related mechanisms responsible for structural changes. We have also observed emission from the fs-modified regions of PMMA and PDMS. An ESR spectrum, recorded a few days after irradiation, from the fs laser-modified regions in PMMA did not reveal any signature of free radicals. However, fs-modified PDMS regions exhibited a single peak in the ESR signal. The probable rationale for the behavior of the ESR spectra in PMMA and PDMS are discussed in the light of free radical formation after fs irradiation. Microchannels within the bulk and surface of PMMA were achieved as well. Microcraters on the surfaces of PMMA and PDMS were also accomplished, and the variation of structure properties with diverse writing conditions has been studied. © 2010 Optical Society of America

OCIS codes: 050.1950, 130.3120, 220.4000, 300.6450.

1. Introduction

Though there are several lithographic techniques with inimitable capabilities, fs laser direct writing (LDW) has been established to be a potential technique for precise structuring of well-defined, three-dimensional submicron features, especially in polymers, because of minimal damage arising from the generation of stress waves, thermal conduction, or melting [1–10]. A variety of materials including metals, dielectrics, polymers, and semiconductors, has been successfully processed by the use of fs pulses

0003-6935/10/132475-15$15.00/0
© 2010 Optical Society of America

[4–10]. When fs pulses are tightly focused into a transparent material, large peak intensities at the focal volume result in nonlinear absorption and ionization (e.g., multiphoton, tunneling, or avalanche type) guiding to an array of changes in material physical and optical properties. These include negative refractive index (RI) change, positive RI change, or simply void formation. This highly controlled modification endows fs LDW a unique two-dimensional/three-dimensional (2D/3D) microfabrication capability without the use of any phase mask or special sample preparation, unlike in other techniques. Polymers, in general, are rapidly forming the basis for a wide range of optical and optoelectronic components and possess several advantages over traditional materials, such as glasses and semiconductors. Optically transparent polymers, particularly poly(methylmethacrylate) (PMMA) and poly(dimethylsiloxane) (PDMS), are now widely used in diverse fields, ranging from microfluidics to optical MEMS, owing to their low cost, processability, and accessibility. Generally, two-photon polymerization is the major mechanism for creation of micro- and nanostructures in various photoresists or polymer resins that are induced by fs laser pulses. Monomers with a lower degree of polymerization can be highly polymerized through this mechanism. Post-exposure treatments are usually needed to realize 3D structures. fs pulses have been widely employed in micromachining bulk polymers, including PMMA and PDMS. This technique has been successfully employed in PMMA to engineer and integrate various optical/photonic and microfluidic structures, such as volume optical data storage [11–14], 2D and 3D gratings [15–22], waveguides [23–26], photonic band gap structures [27–29], microfluidic structures/devices [30–34], and structures for MEMS applications [35]. However, the interaction of laser pulses, particularly ultrashort pulses, with polymers is intricate and requires several complementary techniques to discover the changes occurring on the surface or inside the bulk [36–47]. Several polymers and their doped counterparts have been scrutinized over the last few years for their interaction with fs pulses for potential applications in photonics and microfluidics/optofluidics [48–58]. PDMS is also one of the most widely used flexible polymers for biomedical and biotechnology applications because of its high chemical stability and optical transparency [59–63]. The impulse for such studies, including ours, is to explore the feasibility and identify appropriate experimental conditions for fabricating high-quality optical and microfluidic structures on a single polymer substrate within a single exposure. In this milieu, a comprehensive perception of the fs laser-induced changes is indispensable to identify the appropriate writing conditions for creation of several diverse structures on a single substrate of PMMA and PDMS.

In the present study, we have attempted fabricating several microstructures, such as buried gratings, surface gratings (SG), surface microcraters, and microchannels, in bulk PMMA and PDMS using ~100 fs pulses. A methodical study of the diffraction efficiency (DE) of the achieved gratings was performed as a function of scanning speed, energy, and focal spot size. An optimized set of writing parameters has been identified for achieving efficient volume gratings. The highest DE recorded in the PDMS grating was ~10%, representing an enhancement of 70% with those reported recently [64], and a highest DE of ~34% in the PMMA grating was obtained with a 0.65 NA (40X) objective and single-scan procedure. Raman, UV-visible, electron spin resonance (ESR) spectroscopic methods and laser confocal, scanning electron microscopy (SEM) techniques were utilized to examine the fs laser-modified regions in an endeavor to understand the mechanisms responsible for physical changes at the focal volume. Raman spectra collected from the laser-modified regions of the PMMA indicated bond scission, softening, and stress-related mechanisms responsible for structural changes. We have also observed emission from the fs-modified regions in PMMA and PDMS. An ESR spectrum, recorded a few days after the writing procedure, from the laser-modified regions in PMMA did not reveal any peaks, as reported earlier [13]. Microcraters on the surfaces of PMMA and PDMS were fabricated, and the variation of those structures with writing parameters has been studied. Applications of such structures in photonics and microfluidics are discussed briefly.

2. Experimental Details

The laser source was a Ti:sapphire amplifier operating at 800 nm delivering 1 kHz, ~100 fs pulses with a maximum energy of ~1 mJ. The time-bandwidth product confirmed that pulses were near-transform limited. Three stages, capable of 17 nm resolution, were utilized to translate the sample in the X, Y, and Z directions. High-quality PMMA samples (Goodfellow, USA) of 1 mm thickness (PDMS samples were 6 mm thick) cut into 1 cm × 2 cm pieces were typically used for writing the structures. The energy of the laser was varied using a half-wave plate and a polarizer combination. Writing was performed in the transverse geometry. Typically, pulses with $<2\,\mu$J energy used for writing the structures demonstrated smooth RI change at the focal volume. Structures written with energies ranging from $>2\,\mu$J to ~500 μJ were also studied. The surface of the sample was imaged using a CCD camera to identify position of the focal spot. Surface plasma emission was taken as a reference, and, accordingly, the position of the substrate was adjusted to write structures on or below the surface. Detailed alignment procedures for writing buried structures are presented in our earlier publications [65,66].

We had used 0.65 NA (40X) and 0.4 NA (20X) microscopic objectives in all of our experiments. Spot sizes were calculated using the relation $D = 1.22\lambda/\mathrm{NA}$, where D is the diameter of the focused spot, λ is the wavelength, and NA is the numerical aperture of the microscope objective. The spot sizes were estimated to be ~1.5 and ~2.4 μm, respectively, for 0.65 NA (40X) and 0.4 NA (20X) objectives, respectively. The energy

of an 800 nm photon corresponds to 1.55 eV, while the optical band gap of pure PMMA being 4.58 eV implies that the nonlinear process, involving at least three photons, is responsible for structural modification at the focal volume [19]. In addition to the three photon absorption (3PA) process, Schaffer *et al.* [67] have shown that there are three possible mechanisms (namely, tunneling, intermediate, and multiphoton ionization) that occur when transparent material interacts with fs pulses. For the present studies, the Keldysh parameter was calculated to be <0.5, suggesting tunneling as a possible responsible mechanism for structures written using 0.65 NA (40X) and 0.4 NA (20X) objectives. All the buried structures were located a few hundred microns below the surface. The actual pulse energies at the sample surface were estimated, taking into account the losses during propagation, and transmission losses.

3. Results and Discussion

After optimizing the parameters, such as scan speed and input pulse energy for initial straight-line-like microstructures, we prepared buried gratings, microcraters (on the surface), SG, buried microchannels, and 2D photonic crystal-like structures in PMMA and PDMS with diverse writing conditions. Microstructures were written using single- and double-scan methods, utilizing both 0.65 NA (40X) and 0.4 NA (20X) objectives. For reproducibility, we have obtained two sets of structures in PMMA, and the structure's data (e.g., width, depth, and period) were consistent. Typical separation between the structures was $15/20\,\mu$m, while the widths varied from 3–80 μm, depending on the input energy and scan speeds. We found that the structure width increased with input energy and the number of scans. For structures written at the same energy, structure width was found to be higher in PDMS compared to PMMA, as expected, since PDMS is a relatively soft, rubbery kind of material compared to PMMA, which is harder. For example, the tensile strength of PDMS is ~2.24 MPa, while for PMMA, it is ~70 MPa. We obtained smoother and better quality diffraction gratings (both surface and buried) in PDMS, compared to that of PMMA under similar writing conditions. Figure 1 illustrates the confocal microscopic images of typical structures in PMMA achieved with varying input energies. For structures written with typical energies of $<2\,\mu$J, we confirmed, through confocal, SEM, and Raman spectroscopic studies that the change was purely RI based, without the presence of any voids. For structures written with energies of typically $>2\,\mu$J and $<50\,\mu$J the modification was an RI change combined with voids formation. For structures of $>50\,\mu$J, there was clear indication of empty channel formation within the bulk. Even the empty channels obtained with such high energies enabled us to fabricate grating structures. The RI of bulk PMMA was ~1.49, whereas the RI of the empty channel was assumed to be ~1 (air), enabling sufficient contrast to produce a diffraction pattern. Figures 2(a) to 2(d) depict the cross-sectional SEM images of structures written with different energies. It is evident that for intermediate energies ($>2\,\mu$J and $<50\,\mu$J), hybrid structures were formed, and clear voids for energies were $>50\,\mu$J. Thirteen gratings were fabricated with different writing conditions, such as (a) energy varying from

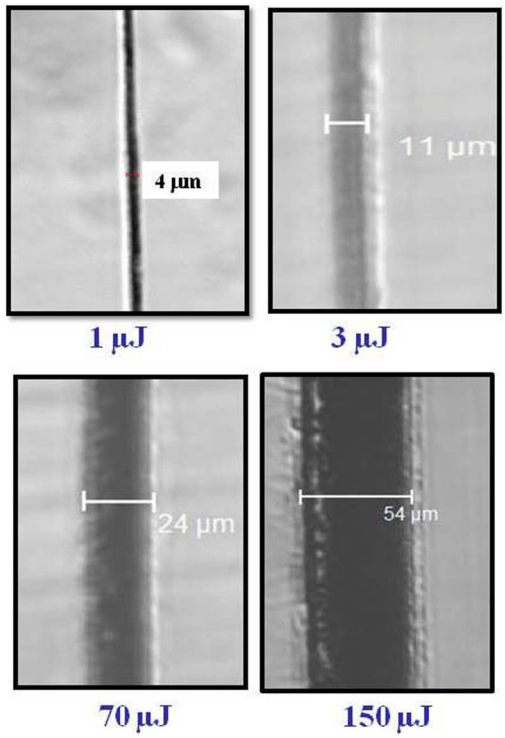

Fig. 1. (Color online) Confocal microscopic images of the microstructures written with a 1 mm/s speed at different energies in PMMA (local grade).

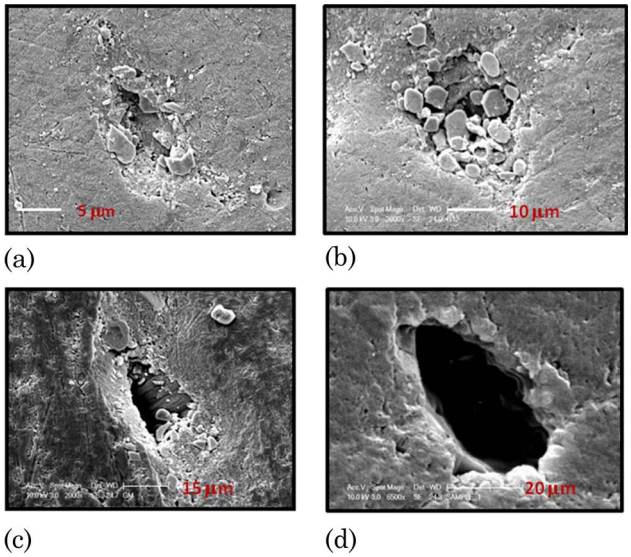

Fig. 2. (Color online) (a) Typical cross section image of a structure captured using SEM written with energy of $<2\,\mu$J, (b) SEM cross-sectional image of a structure written with energy of $\sim 20\,\mu$J, (c) SEM cross-sectional image of structure written with energy of $\sim 40\,\mu$J, and (d) SEM cross-sectional image of structure written with energy of $\sim 75\,\mu$J.

50 μJ to 200 μJ and (b) speeds varying from 0.25 mm/s to 1 mm/s. Five of these thirteen gratings did not exhibit diffraction, owing to overlap of the structures, which was later confirmed through laser confocal imaging studies. The estimated DE ranged from 3.5% to 34%, depending on the writing conditions. The highest DE of ~34% was achieved for the grating written with ~50 μJ energy and 0.25 mm/s scanning speed. This represents one of the highest DE reported in PMMA gratings achieved using fs pulses. Figure 3(a) shows a typical confocal image of the diffraction grating (60 μJ, 0.5 mm/s) achieved using 0.65 NA (40X) objective lens. Figure 3(b) shows the confocal image of a single structure clearly demonstrating the formation of an empty channel within the bulk. Figure 3(c) shows the diffraction pattern obtained using an He–Ne laser.

We had also fabricated six buried gratings using low input energies and the single-scan method by means of different writing conditions in PMMA and PDMS samples. Table 1 summarizes the writing conditions used for all such gratings in PMMA (Goodfellow, USA), the structural parameters that were determined, and the results that were obtained from DE measurements. The nomenclature followed for different gratings is as follows. For example, in PMMABG1, the first four letters indicate the material, BG indicates buried gratings, 1 represents a grating written with particular writing conditions. Typical widths of the structures were 8–10 μm achieved with a writing speed of 0.5 and 1.0 mm/s. A maximum first-order DE (defined as the power in the first order to the input power) of 7.55% was achieved using these conditions in PMMA. Hirono *et al.* [20] reported an increment in the DE of PMMA gratings obtained with 120 fs pulses through heat treatment at 70 °C for 500 hours. Initially, the efficiency recorded was 1.9%, and after heat treatment the efficiency increased to 72%. They argue that the increase was due to the increase in induced RI change after heating and suggested the physical mechanism responsible was volume contraction at the irradiated area. We expected to enhance the efficiency further in our gratings through similar heat treatment and performed the DE studies three times after heating the gratings for >100 h, >200 h, and >300 h. The efficiencies were marginally better than the initial data but within the experimental errors of ±15%. The reason for this could be that the gratings in our case are either of the void type or the hybrid type (void + partial RI change), which were not affected much by the heating. Figure 4(a) shows another typical buried grating in PMMA, while Fig. 4(b) shows the emission, collected in the confocal geometry, from a single structure. The emission was absent in the data collected from the pristine PMMA. The depths of the grating were 20–30 μm, measured from the confocal images of cleaved and polished sample cross sections. Figure 4(c) shows the corresponding diffraction pattern obtained. Figure 4(d) shows the geometry for collecting the emission from a single structure using the confocal technique.

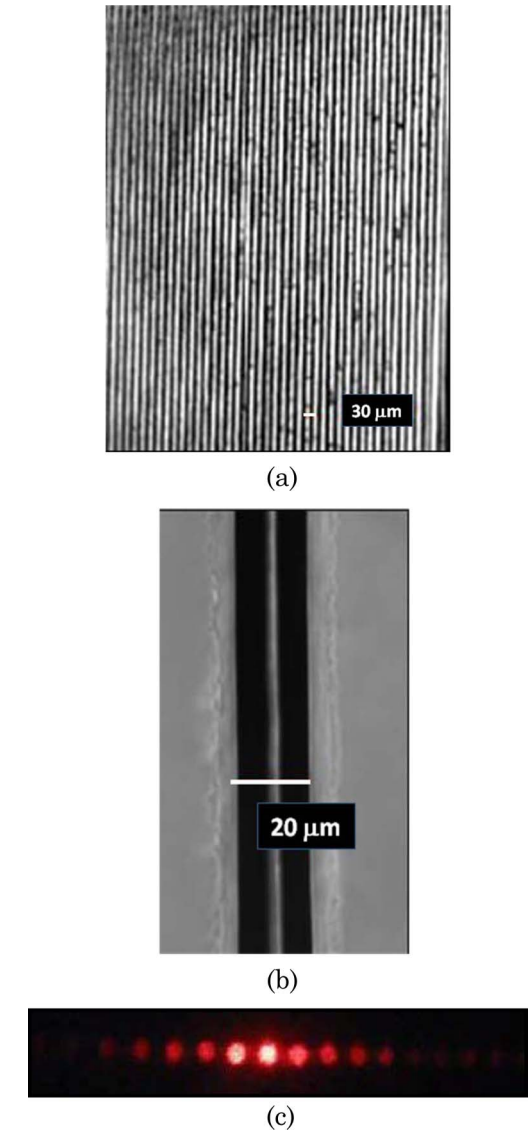

Fig. 3. (Color online) (a) Confocal optical microscopic image of buried grating (~60 μJ, 0.5 mm/s), (b) zoomed optical image of a single structure indicating void/empty channel formed with a width of 20 μm, and (c) diffraction pattern with a first-order efficiency of 20%.

In order to study the modifications that occurred in the exposed regions of PMMA and PDMS, we collected the UV-visible, ESR, Raman, and emission spectra from unexposed and exposed regions of the samples. Figure 5 shows the transmission spectra obtained from modified and unmodified PMMA samples, and the spectra did not reveal any significant changes. PMMA/PDMS do not have significant linear absorption in the visible region. The decrease in transmittance could be attributed to the scattering from the structures or defects induced during the writing process. For collecting the ESR spectra, we had fabricated 2D grids on the PMMA surface using ~3, 6, and 30 μJ energies, a scanning speed of 1 mm/s, and the data were collected after five days, since the spectra had to be recorded at a different institution. Figure 6(a) shows the ESR spectrum of

Table 1. Grating Data Written with Low Energies [0.65 NA (40X) for BG1–BG3 and 0.4 NA (20X) for BG4–BG6] for PMMA (Goodfellow)

Sample	Buried Gratings	Order	Left Side (mW)	Right Side (mW)	Average (mW)	% DE
1	PMMABG1 (~3 μJ,	0		2.5		47.17
	1 mm/s, 15 μm period,	1	0.5	0.3	0.4	7.55
	width 8 μm)	2	0.2	0.1	0.15	2.83
		3	0.1	0.1	0.1	1.89
2	PMMABG2 (~3 μJ,	0		3.6		67.92
	0.5 mm/s, 20 μm	1	0.3	0.2	0.25	4.72
	period, width 10 μm)	2	0.2	0.1	0.15	2.83
		3	0.1	0.1	0.1	1.89
3	PMMABG3 (~6 μJ,	0		3.6		72
	1 mm/s, 20 μm period,	1	0.2	0.3	0.25	5
	width 8 μm)	2	0.2	0.2	0.2	4
		3	0.1	0.1	0.1	2
4	PMMABG4 (~3 μJ,	0		0.2		3.85
	1 mm/s, 15 μm period,	1	0.1	0.1	0.1	1.92
	width 8 μm)	2	0.1	0.1	0.1	1.92
		3		Very weak		
5	PMMABG5 (~3 μJ,	0		0.2		3.77
	0.5 mm/s, 20 μm	1	0.1	0.2	0.15	3.77
	period, width 10 μm)	2	0.1	0.1	0.1	1.89
		3	0.1	0.1	0.1	1.89
6	PMMABG6 (~6 μJ, 1 mm/s, 20 μm period, width 8 μm)			No pattern was observed.		

pristine PMMA, while Fig. 6(b) shows the ESR spectrum of irradiated/modified PMMA with ~30 μJ energy. Figure 6(c) depicts the ESR spectrum of mechanically scratched PMMA, and Fig. 6(d) shows the same spectrum recorded after 1.5 h. There was no ESR signal established [Fig. 6(b)], as we believe the lifetime of free radicals, responsible for the ESR peaks, is too short. We suppose that the free radicals generated during the fs irradiation have transformed into the peroxide radicals, which disappeared after a certain amount of time [68]. Pure PMMA is not a paramagnetic substance and, therefore, cannot contribute toward any peaks in the ESR spectrum. When these polymers are irradiated with ionizing radiation, free radicals are generated. If a polymer is irradiated in a vacuum, the radical concentration produced in the polymer depends on the irradiation dose. When vacuum-irradiated polymers are exposed to air, the radicals trapped in the material are transformed into peroxide radicals by the addition of molecular oxygen to the free radicals. Kaptan and Guven [69] have irradiated PMMA with γ radiation in a vacuum and reported a nine-line ESR spectrum. They also showed that the nine-line spectrum

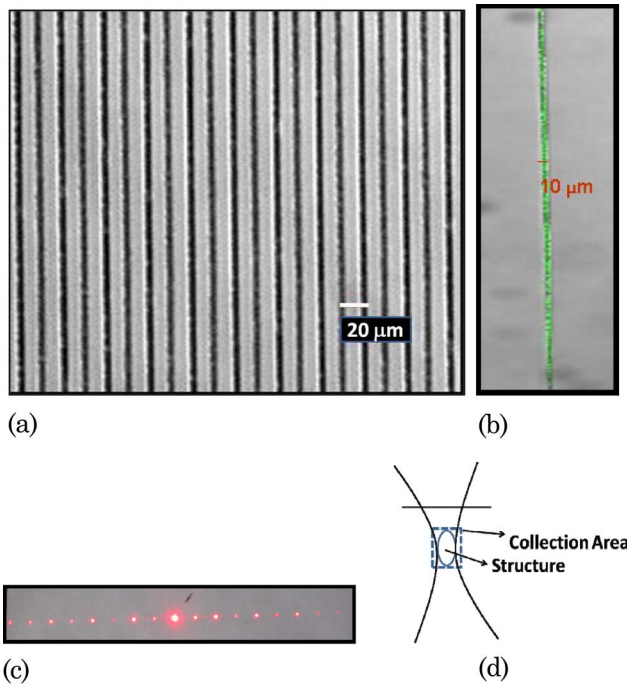

Fig. 4. (Color online) (a) Confocal optical microscope image of grating PMMABG2 (~3 μJ, 0.5 mm/s, 20 μm period, width 10 μm), (b) image of a single structure with emission from the irradiated regions indicated by the pseudo green (gray) color, (c) diffraction pattern from the grating, and (d) geometry used in collecting the emission from the structures.

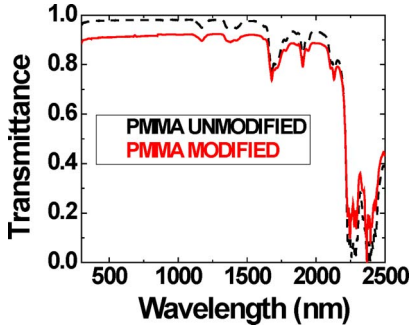

Fig. 5. (Color online) Transmission spectra recorded for PMMA grating (50 μJ, 0.25 mm/s). The dashed curve represents the unmodified PMMA, while the solid curve represents the laser-modified PMMA.

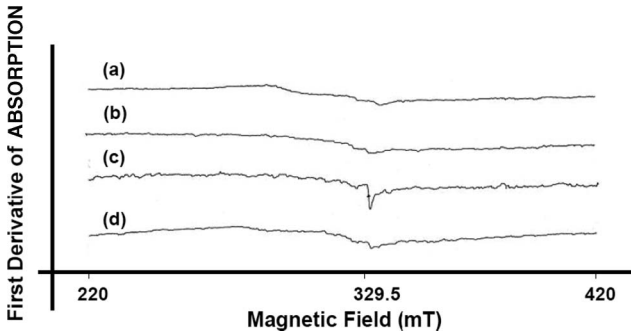

Fig. 6. ESR data from the (a) unmodified regions of PMMA, (b) fs laser-modified PMMA, (c) physically scratched PMMA recorded immediately, and (d) after 90 min.

changed to a single-peak spectrum when exposed to air, due to the formation of an antisymmetric peroxide radical. Kaptan and Tatar [70] accounted that the observed nine-peak ESR spectrum in mechanically fractured PMMA was also strongly temperature dependent. Szocs [71] had shown the same characteristic nine-line ESR spectrum of PMMA irradiated with x rays. Velter-Stefanescu *et al.* [72] have collected ESR spectra for electron-irradiated PMMA and an observed signal (single peak) at 326.5 *milliTesla* (mT). Mechanically scratched PMMA depicts a single-peak ESR signal, due to an antisymmetric peroxide radical resulting from mechanoradicals that were generated during the process. Nie *et al.* [13] revealed the same nine-line ESR spectrum obtained from an fs-modified PMMA immediately after irradiation and envisaged the reason for observation was free radical generation. However, we expect to achieve the nine-line spectrum in the near future, when the ESR will be recorded immediately after exposure.

A typical Raman spectra recorded from buried PMMA structures is depicted in Fig. 7(a) for higher energies (~50 μJ) and 7(b) for lower energies (~3 μJ). It is evident from Fig. 7(a) that various peaks in the spectrum collected from the fs-modified regions were broadened drastically, probably due to the huge strain created by the enormous peak intensities, and thereby the shock waves created, at focal volume. It is possible that broadening of Raman peaks could result from pressure-driven structural disordering at high energies. SEM images of these structures confirmed formation of voids/empty channels [see, e.g., Fig. 2(c)]. The debris from the voids region is redeposited, which contributes to the Raman signals. Raman spectra collected from regions far away from the focal volume (unmodified regions) did not reveal any peak broadening. Figure 7(b) shows the Raman spectrum from low energy laser-irradiated (low energy of ~3 μJ) regions, which clearly indicate that the changes are minute to the peak widths, unlike in the high-energy case. The Raman spectrum collected from the irradiated regions clearly suggested slight broadening of the peak near 1500–1750 cm^{-1}, indicating that the stress formed during irradiation. There have been

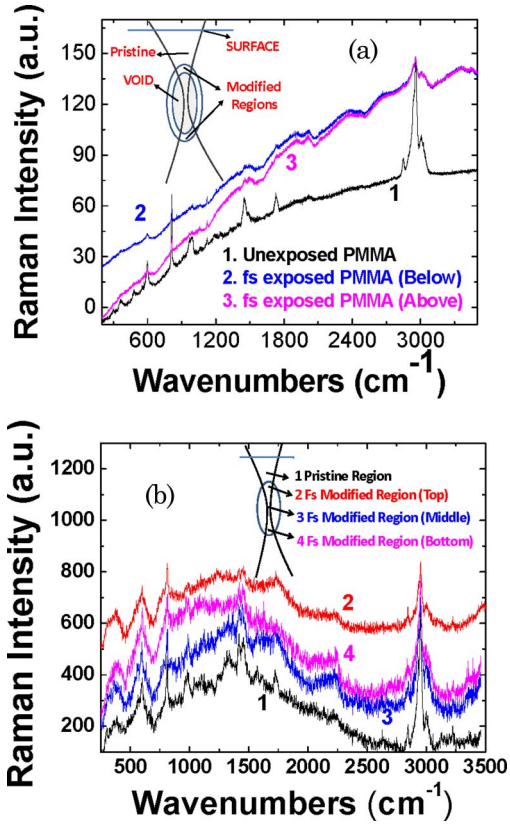

Fig. 7. (Color online) (a) Raman spectra from a PMMA grating (50 μJ, 0.25 mm/s) with the bottom curve representing the spectrum collected from unmodified regions of PMMA while the middle and top curves from the fs-modified regions. (b) Micro-Raman spectrum of PMMABG2 grating (~3 μJ, 500 μm/s) achieved with 0.65 NA (40X) objective. The curves have been shifted for clarity. Inset shows the regions from which the spectra were collected.

few studies reported in the literature for exploring the RI change in PMMA using fs pulses [17–20,47]. Mochizuki *et al.* [40] studied a variety of polymers for possible mechanisms for fs laser interaction. They fabricated gratings in PMMA with 120 fs pulses and achieved DE <5%. The RI change observed using fs irradiation was mainly from density changes, although other processes, such as structural changes,

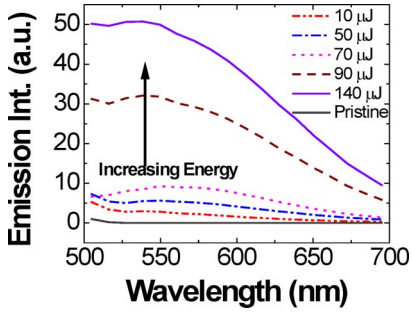

Fig. 8. (Color online) PMMA emission data collected from the fs-modified regions with excitation at 488 nm and increasing energies. The bottom curve represents the data collected from pristine PMMA. Structures were obtained with 0.65 NA (40X) objective lens and 1 mm/s scanning speed with different energies.

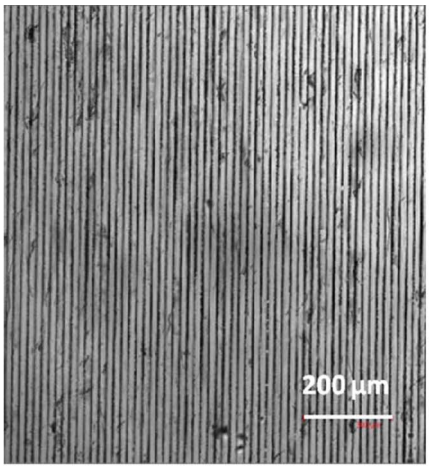

(a)

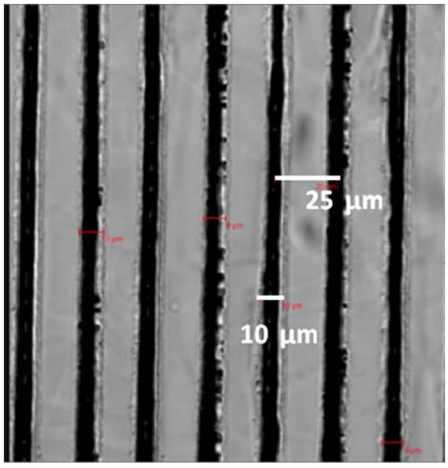

(b)

(c)

Fig. 9. (Color online) (a) Laser confocal images of SG in PMMASG2 and their corresponding diffraction images. Scale bar in (a) is 200 μm. Energy used was ~6 μJ, writing speed of 1 mm/s, width 10 μm, and spacing 25 μm with 0.65 NA (40X) objective, (b) magnified view of the grating, and (c) diffraction pattern from the grating.

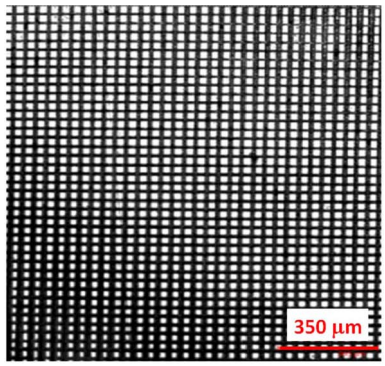

(a)

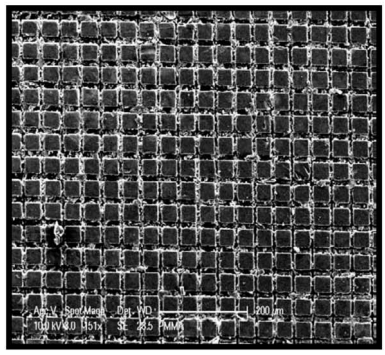

(b)

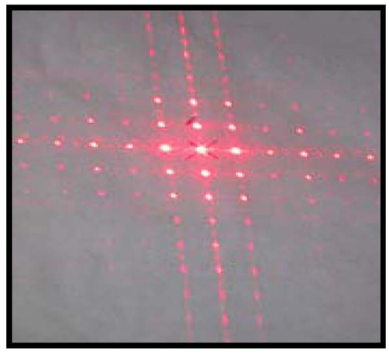

(c)

Fig. 10. (Color online) (a) Laser confocal images of 2D SG in PMMASG3 (Goodfellow) using 0.65 NA (40X) objective (scale bar is 350 μm), (b) corresponding SEM image of the 2D SG (scale bar is 200 μm), and (c) diffraction pattern observed from the grating: energy used was <25 μJ, writing speed of 1 mm/s, width 22 μm, and spacing was 35 μm with 40 X objective.

could also affect the RI change. Baum *et al.* [18,19] reported that the RI increase was due to the complete and partial separation of the side chain from the PMMA molecule. Another report by Watanabe *et al.* [23] claims tensile stress also is responsible for the RI change. Wochnowski *et al.* [17] through their studies assert that benzene rings in the polymer main chain are activated by multiphoton absorption; therefore, the benzene rings are cleaved from the rest of the polymer molecule, followed by the total defragmentation of the benzene rings themselves.

The fs-modified regions of PMMA, excited at a wavelength of 488 nm, exhibited strong emission near spectral regions of ~540 nm. The emission was collected in the confocal geometry from laser-modified regions [as described in Fig. 4(d)]. Figure 8 depicts the emission collected from modified regions with varying input energies used for writing the structures. That the emission intensity increased with increasing input energy used is evident from the figure. This behavior could be attributed to either of (a) an increase in the actual structure width/area and, hence, the overall emission signal or (b) the PMMA interaction/modification being different with increasing energies and, therefore, the change in emission intensity. We contemplate the observed

Table 2. Data for Surface Gratings in Bulk PMMA (Goodfellow) and Bulk PDMS Written with 0.65 NA (40X) Objective

SG	Energy (~μJ)	Period (μm)	Speed (mm/s)	Width (μm)	Zeroth Order % DE	First Order % DE	Second Order % DE	Third Order % DE
PMMASG1	3	18	1	9	1.83	0.83	0.3	0.17
PMMASG2	6	25	1	10	46.83	5.83	2.17	0.83
PMMASG3	30	35	1	22	45.67	4.66	0.66	1.42
PDMSSG1	3	12	1	8	4.59	2.6	1.4	0.57
PDMSSG2	6	30	1	15	32.73	9.6	0.66	0.74
PDMSSG3	30	65	1	30	34	7.7	2.22	0.49

emission could be from the defects generated due to bond scission of PMMA [13]. However, further detailed studies are necessary to identify the exact cause for this emission. There are sparse reports on the observation of emission from fs laser-modified PMMA. Nie *et al.* [13] reported multilayered optical bit memory in fluorescent PMMA irradiated with fs pulses. They observed fluorescence in fs-irradiated PMMA when excited at 442 nm and attribute it to the defects generated by bond scission. The excitation spectrum in their case had a peak near 360 nm. Formation of color centers in our case is ruled out, since the absorption/transmission spectra recorded before and after irradiation did not display any additional peaks in the visible region [73]. The reason for emission from fs-modified PMMA due to the free radicals is also ruled out, since the emission was observed even a few months after exposure.

We also achieved SG in PMMA with different input energies. We investigated the quality of these gratings and compared their performance with those of

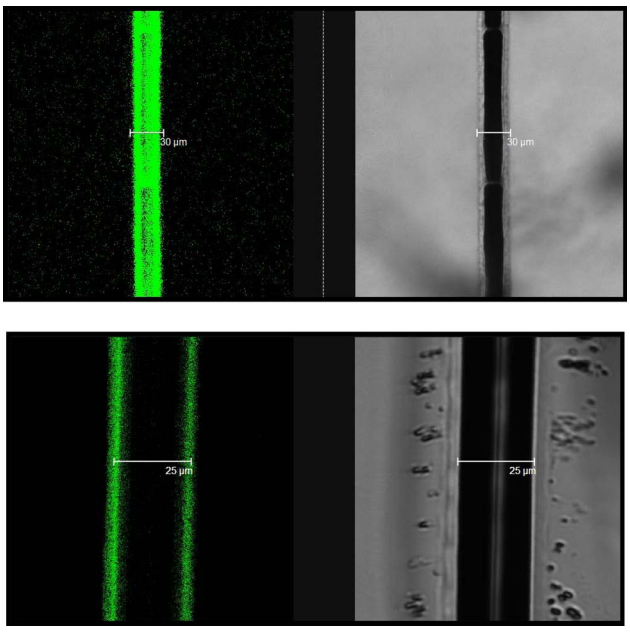

Fig. 11. (Color online) (a) Laser confocal images of ~20 μm wide buried microchannel in PMMA (30 μJ, 1 mm/s) and 0.65 NA (40 X) focusing. The length of the scale bar is 30 μm. (b) Typical ~25 μm wide microchannel on the surface of PMMA (30 μJ, 1 mm/s) and 0.65 NA (40 X) focusing. Pseudo color (green) indicates the emission from the laser-modified regions. The length of the scale bar is 25 μm.

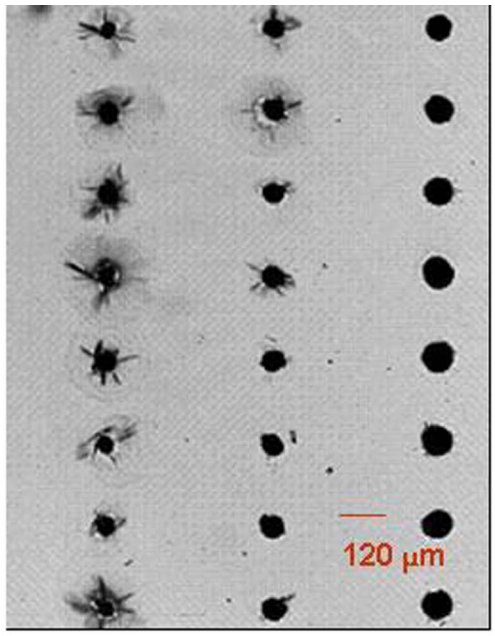

(a)

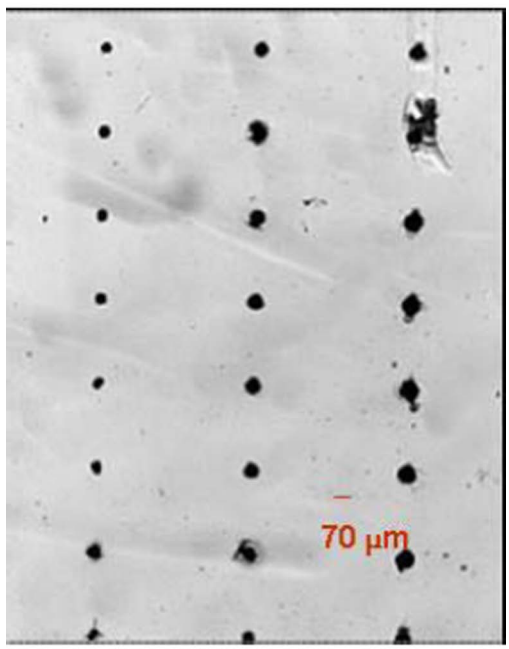

(b)

Fig. 12. (Color online) Microcraters on the surface of PMMA with (a) 0.4 NA (20 X) focusing and (b) 0.65 NA (40 X) focusing. Left to right rows: 10, 20, and 50 μJ, top to bottom: 5 s to 50 s in steps of 5 s exposure time.

buried gratings. Figures 9 and 10 depict typical gratings achieved on the PMMA surface. Table 2 illustrates SG written with 0.65 NA (40X) objective in PMMA and PDMS (PMMASG 1 to PMMASG3 and PDMSSG1 to PDMSSG3). PMMASG1 had a DE of 0.83%, while the buried counterpart grating PMMABG1 (similar writing conditions) had a DE of 7.55%, probably due to better RI contrast in the latter case. The debris collected on the SG could have influenced the reduction of the RI contrast. However, PMMASG2 (~6 μJ, 1.0 mm/s) had a DE of 5.83%—better than the DE of PMMABG2 (~3 μJ, 0.5 mm/s), which was 4.72%. With the identical conditions used for writing SG, 2D crossed gratings (one set of structures and another set written perpendicular to the first one) were also attempted. Figures 10(a) and 10(b) display confocal and SEM images of such crossed gratings in PMMA, and 10(c) depicts the diffraction pattern, from the grating shown in 10(b) observed in the far field. At least 6–7 orders on either side of the main transmitted beam were observed for all the gratings fabricated.

Figure 11(a) shows the confocal images of a typical microchannel achieved within the bulk, and Fig. 11(b) illustrates the confocal images of a typical channel on the surface of PMMA achieved with ~30 μJ input energy. For the buried case, the channel width was ~20 μm, slightly lower than that of the surface channel. Confocal images indicate the emission (pseudo color of green) presence from only the fs-modified regions surrounding the structures in both cases, undoubtedly evident in the surface structure. In the buried channel case, the emission was collected from the top of the surface, which is from the whole channel. For the case of surface structures, the material was ejected from the fs laser-exposed region, creating a dip (crater) with the debris clearly deposited in the nearby surface regions. The width of this structure was ~25 μm achieved with 0.65 NA (40X) objective and a scanning speed of 1 mm/s. The typical length of buried channels was ~1 cm, while the present technique is capable of creating even longer channels. The roughness/smoothness in these channels could be reduced/improved by means of (a) fabricating them with continuous water flow or inserting the sample inside water [31] or (b) using a multiple scanning method. Figure 12 illustrates the craterlike structures on the surface of PMMA and PDMS with 0.65 NA (40X) focusing conditions. The exposure time varied from 5 s to 50 s in steps of 5 s (10 craters). For the rows right to left, the energy varied as 50 μJ (column 3), 20 μJ (column 2), and 10 μJ (column 1). Typical structure width (diameter of the crater) varied from 50 μm to 100 μm. The structures resulting from 0.4 NA (20X) objective were definitely larger in diameter than those exposed with 0.65 NA (40X) objective, since the focused spot size was larger in the former case. The depths of structures obtained with 0.65 NA (40X) could be higher compared to structures obtained with 0.4 NA (20X) focusing. SEM studies are in progress to determine exactly the dimensions in each case. The appearance of cracks in structures obtained with 0.4 NA (20X) and at small exposure times is puzzling and requires further work to understand the reasons for their occurrence. The position of the focal volume could be different in each case, resulting in a higher ablation rate and thereby induce cracks. The results from such studies support us in fabricating microchannels and reservoirs, which are the building blocks for lab-on-a-chip devices.

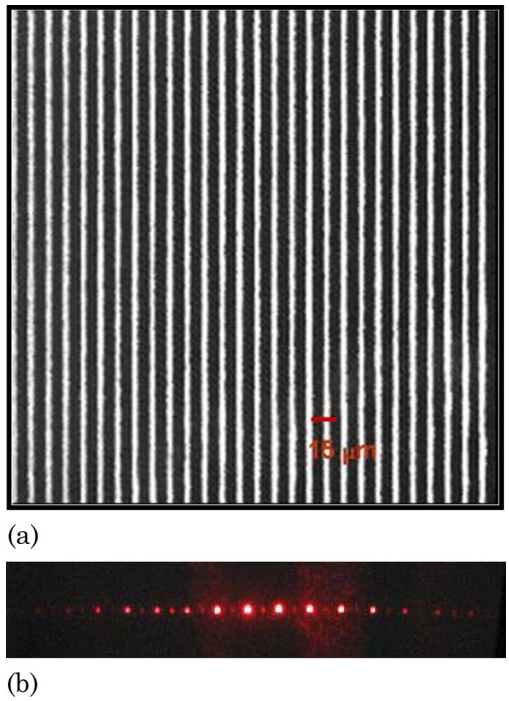

Fig. 13. (Color online) (a) Grating in PDMSBG1 with a structure width of 8 μm and spacing of 15 μm. The scale bar length is 15 μm. (b) Diffraction pattern.

Table 3. Summary of the Structures Written in PDMS Using Both 0.65 NA (40X) and 0.4 NA (20X) Objectives[a]

Buried Gratings	Energy (~μJ)	Speed (μm/s)	Per. (μm)	Width (μm)	Depth (μm)	% DE Zeroth Order	% DE First Order	% DE Second Order	$\Delta n(\times 10^{-3})$
PDMSBG1	3	1000	15	9	34	18.3	10	1.66	1.94
PDMSBG2	3	500	20	13	20	9.24	7.7	3.1	2.87
PDMSBG3	5	1000	20	16	26	5	5	1.66	1.76
PDMSBG4	3	1000	15			No grating formed			
PDMSBG5	3	500	20	14	10	4.61	3.18	1.86	3.50
PDMSBG6	5	1000	20			No grating formed			

[a]The highest DE recorded for PDMSBG1 was ~10%.

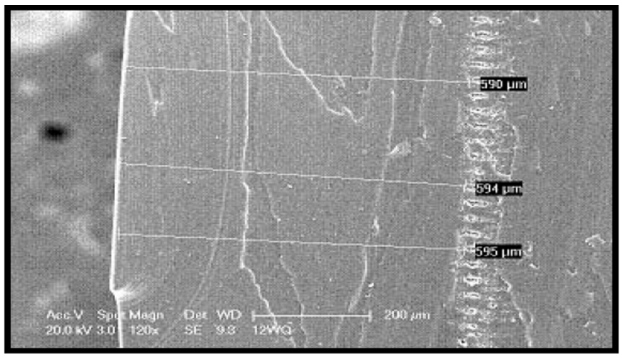

(a)

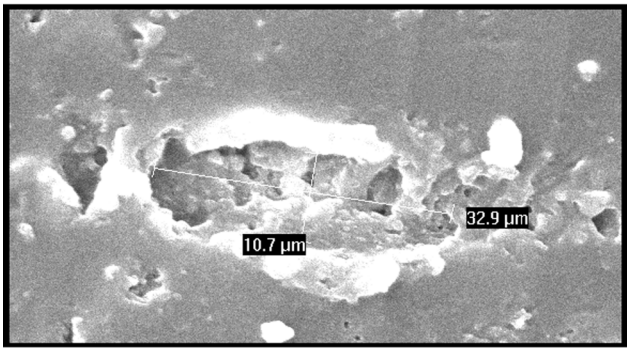

(b)

Fig. 14. (a) SEM picture of PDMSBG1 grating and the modified region (595 μm below the surface) and (b) SEM picture of cross-sectional view of a typical microstructure.

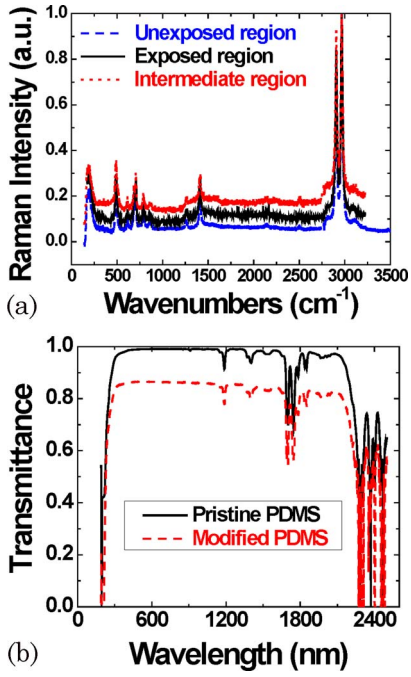

Fig. 15. (Color online) (a) Raman spectra of modified and unmodified regions of PDMSBG3 and (b) transmission spectra of modified and unmodified regions of PDMSBG3.

For PDMS samples, line structures were written at different energies with a scanning speed of 1 mm/s. Figure 13(a) depicts the confocal image of a typical grating structure written with 0.65 NA (40X) objective. Typical separation between the structures was 10–20 μm, while the widths varied from 15–25 μm, depending on the input energy and scan speeds. Similar to PMMA structures, we identified that the structures written with energies of <3 μJ resulted in a smooth RI change (confirmed through SEM cross-sectional images), and energies used in the 3 μJ–30 μJ range resulted in complicated/hybrid structures (RI modified regions surrounding the void regions). For energies of >30 μJ dumped at the focal volume, complete voids were formed. We had fabricated six gratings (PDMSBG1 to PDMSBG6) using a single-scan method with different writing conditions in a single PDMS substrate. The structural widths of PDMSBG1, PDMSBG2, and PDMSBG3 were ~9, 13, and 16 μm, confirmed through the confocal data. PDMSBG4, PDMSBG5, and PDMSBG6 were accomplished with similar writing conditions to PDMSBG1, PDMSBG2, and PDMSBG3, except that a 0.4 NA (20X) objective was used. We observed diffraction orders ranging from 8 to 12 for all the gratings. We calculated the DE at 633 nm with an He–Ne laser. The first-order DE (defined as the ratio of power diffracted into the first-order of the input power) of PDMSBG1, PDMSBG2, and PDMSBG3 were 10%, 7.7%, and 5%, respectively, while the second-order DE were 1.66%, 3.1%, and 1.66%, respectively. These correspond to an enhancement in first-order efficiency by ~70% compared to that reported by Cho *et al.* [64]. They had obtained a maximum DE of 6% for the first order, 1.9% for the second order, and 0.5% for the third order. They employed tighter focusing conditions (0.85 NA), while we used a 0.65 NA (40X) objective. We have also tried fabricating the gratings with a 0.4 NA (20X) objective with similar conditions (energy and speed) to understand the structure's behavior with varying focal situations. For the case of PDMSBG4 and PDMSBG6, we could not observe any diffraction pattern due to mixed-up structures due to increased width, later confirmed through confocal images. However, for the case of PDMSBG5, we observed a good diffraction pattern and the efficiency calculated was 3.18%. Gratings written with larger spacing and using a 0.4 NA (20X) objective lens were achieved recently, and our recent optical studies point toward lower DE compared to PDMSBG1, PDMSBG2, and PDMSBG3. These data suggest that the optimal focusing conditions were achieved with a 0.65 NA (40X) objective. Baum *et al.* [18,19] reported DE of 10% in PMMA obtained with ~110 f s pulses, but with 10 repeated scans. They noticed that as the pulse width decreased, the efficiency of the gratings increased, with the best efficiency of 35% obtained for gratings written with 45 f s pulses and 14 repeated scans. Similarly, for PDMS, we expect to enhance the DE further through (a) repeated scans and (b) utilizing even shorter pulses. PDMSBG3 (~5 μJ, 1.0 mm/s) had a DE of 5%, while the corresponding SG PDMSSG2 (~5 μJ, 1.0 mm/s) had a DE of 9.6%, clearly suggesting that the RI contrast is higher in the latter case.

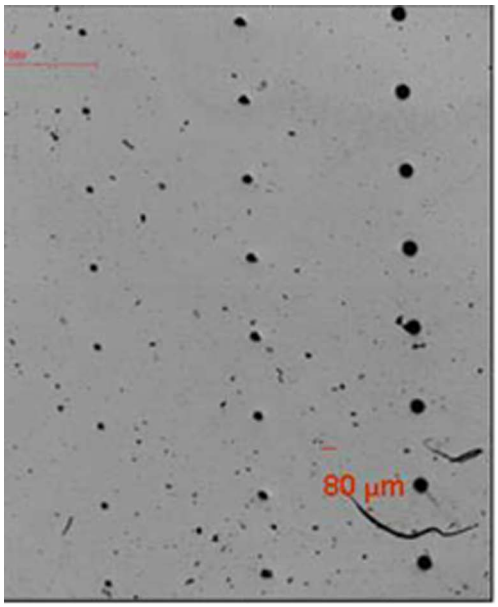

(a)

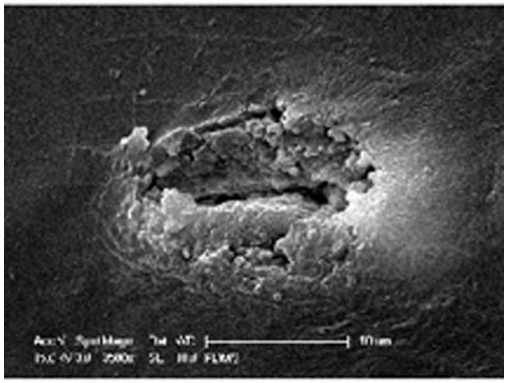

(b)

Fig. 16. (Color online) (a) Surface structures in PDMS using 0.65 NA (40 X) objective. Left to right rows: 10, 20, and 50 μJ; top to bottom: 5 s to 50 s in steps of 5 s exposure time. (b) SEM image of a typical microcrater structure on the surface of PDMS.

The depths of buried gratings PDMSBG1, PDMSBG2, and PDMSBG3, measured from SEM images, were 34, 20, and 26 μm, respectively. We calculated the RI changes (assuming that a smooth variation though the SEM images indicates the presence of small voids) for PDMSG1, PDMSG2, and PDMSG3 to be $\sim 1.9 \times 10^{-3}$, $\sim 2.9 \times 10^{-3}$, and $\sim 1.8 \times 10^{-3}$, respectively [17]. Similar calculations were performed for PDMSG5. These values were calculated from the DE data and structural parameters, such as the depth of the grating [17]. There could be an error of $\pm 20\%$ in the RI change estimates arising from uncertainties in depth measurements and DE calculations. Table 3 summarizes the data obtained for all gratings studied. To gain knowledge about the physical changes in the laser-modified region, we cut the sample transversely, polished, and coated it with gold for conduction and viewed the structures with SEM. The result presented in Fig. 14(a) portrays the depth of structures from the surface, and Fig. 14(b) illustrates the cross-sectional SEM image of a sliced structure. It is evident from these pictures that the gratings were formed $\sim$400–600 μm below the surface, and the depth of the gratings varied from 20 to 30 μm. The pictures also ascertain, to an extent, that the physical changes, such as localized heating, melting, and resolidification at the focal volume (leading to higher density), are the mechanism responsible for RI change. To further investigate the modified regions, we collected the Raman and UV-visible absorption spectra. Figure 15(a) demonstrates the micro-Raman spectra collected for grating PDMSBG3 from the unexposed region (dashed curve), exposed region (solid curve), and the central regions (dotted

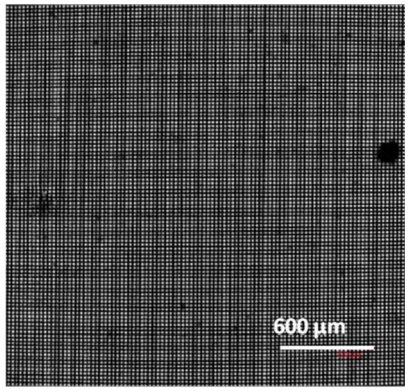

(a)

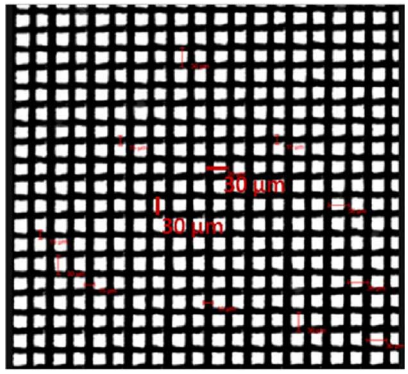

(b)

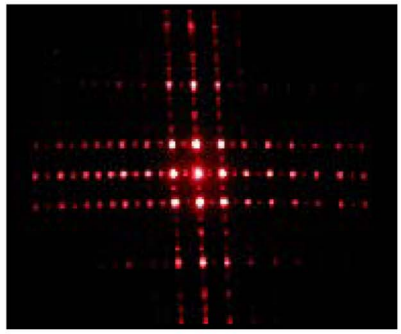

(c)

Fig. 17. (Color online) (a) and (b) Typical 2D grating written in PDMS and (c) corresponding diffraction pattern. Scale bar in (a) is 600 μm, and typical period in (b) is 30 μm.

curve). It is apparent that there is no alteration in the peak positions and widths in different spectral regions. A slight change in Raman intensity of the modified regions compared to unmodified regions was noticed. This data probably suggest that there are no major chemical alterations to the polymer at the focal volume. From the transmission spectra recorded, shown in Fig. 15(b), we could not establish major differences between modified and unmodified regions, except for a shift in the intensity, which could possibly transpire due to scattering from the modified regions. Figure 16(a) shows the microcraters created on the surface of PDMS using 0.65 NA (40X) objective lens with exposure times as explained for the case of PMMA. Figure 16(b) shows a typical SEM image of one such microhole, elucidating the structure formed through high-intensity pulses. The enormous strain created by the short pulse(s) is evident through the fine cracks. The crater was not well-defined, since the debris has settled back imperfectly after the pulse has left. Fabricating such structures in conjunction with the flow of a liquid might reduce the debris and produce a well-defined crater, useful for microfluidic studies. Figures 17(a) and 17(b) show the confocal images of a typical 2D grating on the surface, and Fig. 17(c) shows the clear optical diffraction pattern obtained, indicating a high-quality structure. Figure 18 shows the ESR spectra of pristine PDMS, fs-modified PDMS, and mechanically scratched PDMS. To the best of our knowledge, this is the first report on the ESR spectra of fs-modified PDMS. We have observed one peak near 330 mT in the ESR spectra of fs-modified PDMS, representative of the presence of free radicals. The ESR signal was long-lived from the fs-modified region, since we could observe the peaks in the spectrum collected even after five days. However, unlike in PMMA, the mechanically surface scratched PDMS did not show any ESR peak, suggesting that no mechanoradicals were generated. Interestingly, since the mechanically scratched PMMA and fs laser-modified PDMS exhibited ESR peaks at similar magnetic field and their "g" values were ~1.9, we suppose that same

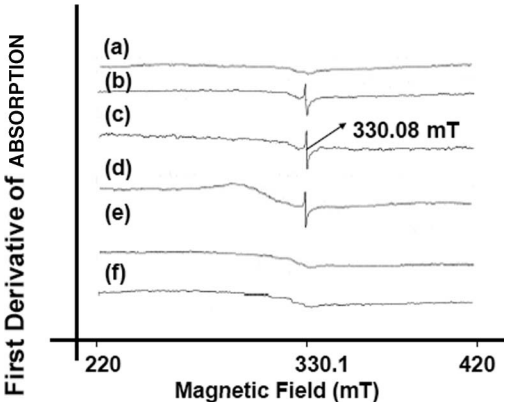

Fig. 18. ESR spectra collected from (a) pristine PDMS, (b)–(d) fs-irradiated PDMS with 3, 6, and 30 μJ energies, respectively, (e) mechanically scratched PDMS immediately, and (f) mechanically scratched PDMS after 15 minutes.

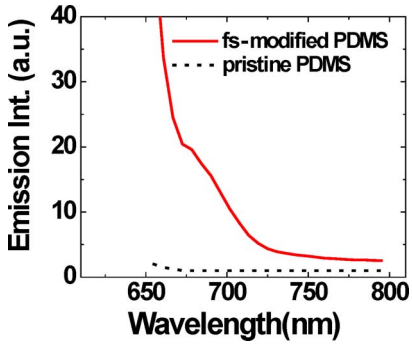

Fig. 19. (Color online) Emission intensity collected from the fs-modified regions of PDMS with excitation at 633 nm. Structures were obtained with 0.65 NA (40 X) objective lens, 1 mm/s scanning speed, and energy of ~18 μJ.

free radical could be responsible for peaks in both the ESR spectra. However, lifetimes are expected to be different for PMMA and PDMS because the host environment is different. Figure 19 shows the emission spectrum from the fs-modified and pristine regions of PDMS, collected immediately after irradiation, with an excitation wavelength of 633 nm. The cause of such an emission could be from the defects generated during exposure, similar to the PMMA case. Further studies are in progress to identify the exact mechanism.

Since the RI change of ~10^{-3} can be accomplished in both PMMA and PDMS, these materials have potential for passive waveguide applications. Our future studies also include (a) improvising the writing conditions further (such as multiple scans) to achieve photonic structures with enhanced efficacy, (b) fabricating waveguides with low propagation loss in both PMMA and PDMS and extracting their 3D RI profiles, (c) fabricating microchannels within the bulk and integrating them with waveguides and other passive optical components for device applications, (d) exploring further the mechanism responsible for ESR behavior, (e) examining the time-dependent emission observed from these structures, (f) fabricating 2D photonic crystals in the bulk of PMMA and PDMS, and (g) integrating simple photonic structures in PMMA and PDMS.

4. Conclusions

We have successfully fabricated several buried and surface microstructures in PMMA and PDMS using fs laser pulses. Multiphoton and tunneling ionization were the probable mechanisms identified for the structural changes at the focal volume. We achieved highly efficient, buried gratings in the bulk of PDMS using fs pulses. A highest first-order DE of ~10% was achieved in the grating written with 0.65 NA (40X) objective (~6 μJ, 1 mm/s). This symbolizes an increase of ~70% over the previously reported similar structures in PDMS. Gratings fabricated with different focusing conditions suggest that the best gratings were achieved with 0.65 NA (40X) focusing. A highest DE of 34% was recorded for one of the PMMA gratings. Confocal and SEM techniques were employed to physically examine the laser-modified regions.

Raman, UV-visible absorption, ESR, and confocal fluorescence spectroscopic techniques were utilized to understand the mechanism responsible for changes at the focal volume. Emission from fs-modified regions of PMMA and PDMS was observed. ESR spectra (collected five days after the fs exposure) from PMMA did not show any peaks. ESR spectrum of fs-modified PDMS, reported for the first time, to the best of our knowledge, exhibited one peak. Fabrication of such high-quality and efficient photonic structures, along with the possibility of creating other optofluidic structures, enhances the prospects of PMMA and PDMS for biomedical applications.

Financial support from the Department of Science and Technology, India, through project SR/S2/LOP-11/2005, is gratefully acknowledged. D.N. Rao and S.V. Rao acknowledge financial support from the Council of Scientific and Industrial Research (CSIR), India. KLND acknowledges the senior research fellowship from CSIR, India. Acknowledgments are also due to C. Yang, Caltech University, for providing the PDMS sample. We gratefully acknowledge J.L. Rao, Sri Venkateswara University, Tirupathi, India for his guidance in the ESR measurements. We acknowledge P.S.R. Prasad, National Geophysical Research Institute, India, for providing support with the micro-Raman measurements. We acknowledge R.S.S. Kumar for his support in the initial part of the experiments and his feedback. We acknowledge partial financial support from ACRHEM, University of Hyderabad.

References

1. H. Becker and C. Gärtner, "Polymer microfabrication technologies for microfluidic systems," Anal. Bioanal. Chem. **390**, 89–111 (2008).
2. Y. Xia, J. A. Rogers, K. E. Paul, and G. M. Whitesides, "Unconventional methods for fabricating and patterning nanostructures," Chem. Rev. **99**, 1823–1848 (1999).
3. B. D. Gates, Q. Xu, M. Stewart, D. Ryan, C. G. Willson, and G. M. Whitesides, "New approaches to nanofabrication: molding, printing, and other techniques," Chem. Rev. **105**, 1171–1196 (2005).
4. R. R. Gattass and E. Mazur, "Femtosecond laser micromachining in transparent materials," Nat. Phot. **2**, 219–225 (2008).
5. S. Juodkazis, V. Mizeikis, and H. Misawa, "Three-dimensional microfabrication of materials by femtosecond lasers for photonics applications," J. Appl. Phys. **106**, 051101 (2009).
6. S. Nolte, M. Will, J. Burghoff, and A. Tuennermann, "Femtosecond waveguide writing: a new avenue to three-dimensional integrated optics," Appl. Phys. A **77**, 109–111 (2003).
7. S. Juodkazis, V. Mizeikis, S. Matsuo, K. Ueno, and H. Misawa, "Three-dimensional micro- and nano-structuring of materials by tightly focused laser radiation," Bull. Chem. Soc. Jpn. **81**, 411–448 (2008).
8. M. Ams, G. D. Marshall, P. Dekker, M. Dubov, V. K. Mezentsev, I. Bennion, and M. J. Withford, "Investigation of ultrafast laser-photonic material interactions: challenges for directly written glass photonics," IEEE J. Sel. Top. Quantum. Electron. **14**, 1370–1381 (2008).
9. J. Qiu, K. Miura, and K. Hirao, "Femtosecond laser-induced microfeatures in glasses and their applications," J. Non-Cryst. Solids **354**, 1100–1111 (2008).
10. G. Della Valle, R. Osellame, and P. Laporta, "Micromachining of photonic devices by femtosecond laser pulses," J. Opt. A: Pure Appl. Opt. **11**, 013001 (2009).
11. E. N. Glezer, M. Milosavljevic, L. Huang, R. J. Finlay, T. H. Her, J. P. Callan, and E. Mazur, "Three-dimensional optical storage inside transparent materials," Opt. Lett. **21**, 2023–2025 (1996).
12. B. H. Cumpston, S. P. Ananthavel, S. Barlow, D. L. Dyer, J. E. Ehrlich, L. L. Erskine, A. A. Heikal, S. M. Kuebler, I. Y. S. Lee, D. McCord-Maughon, J. Q. Qin, H. Rockel, M. Rumi, X. L. Wu, S. R. Marder, and J. W. Perry, "Two-photon polymerization initiators for three dimensional optical data storage and microfabrication," Nature **398**, 51–54 (1999).
13. Z. Nie, H. Lee, H. Yoo, Y. Lee, Y. Kim, K.-S. Lim, and M. Lee, "Multilayered optical bit memory with a high signal-to-noise ratio in fluorescent polymethylmethacrylate," Appl. Phys. Lett. **94**, 111912 (2009).
14. H. Tang, H. Jiu, B. Jiang, J. Cai, H. Xing, Q. Zhang, W. Huang, and A. Xia, "Three-dimensional optical storage recording by microexplosion in a doped PMMA polymer," Proc. SPIE **5643**, 258–263 (2005).
15. D. A. Higgins, T. A. Everett, A. F. Xie, S. M. Forman, and T. Ito, "High-resolution direct-write multiphoton photolithography in poly(methyl methacrylate) films," Appl. Phys. Lett. **88**, 184101 (2006).
16. P. J. Scully, D. Jones, and D. A. Jaroszynski, "Femtosecond laser irradiation of polymethylmethacrylate for refractive index gratings," J. Opt. A: Pure Appl. Opt. **5**, S92–S96 (2003).
17. C. Wochnowski, Y. Cheng, K. Meteva, K. Sugioka, K. Midorikawa, and S. Metev, "Femtosecond-laser induced formation of grating structures in planar polymer substrates," J. Opt. A: Pure Appl. Opt. **7**, 493–501 (2005).
18. A. Baum, P. J. Scully, M. Basanta, C. L. P. Thomas, P. R. Fielden, N. J. Goddard, W. Perrie, and P. R. Chalker, "Photochemistry of refractive index structures in poly (methyl methacrylate) by femtosecond laser irradiation," Opt. Lett. **32**, 190–192 (2007).
19. A. Baum, P. J. Scully, W. Perrie, D. Jones, R. Issac, and D. A. Jaroszynski, "Pulse-duration dependency of femtosecond laser refractive index modification in poly (methyl methacrylate)," Opt. Lett. **33**, 651–653 (2008).
20. S. Hirono, M. Kasuya, K. Matsuda, Y. Ozeki, K. Itoh, H. Mochizuki, and W. Watanabe, "Increasing DE by heating phase gratings formed by femtosecond laser irradiation in poly (methyl methacrylate)," Appl. Phys. Lett. **94**, 241122 (2009).
21. S. Katayama, M. Horiike, K. Hirao, and N. Tsutsumi, "Structures induced by irradiation of femtosecond laser pulse in polymeric materials," J. Polym. Sci. Polym. Phys. **40**, 537–544 (2002).
22. S. Katayama, M. Horiike, K. Hirao, and N. Tsutsumi, "Structure induced by irradiation of femtosecond laser pulse in dyed polymeric materials," J. Polym. Sci. Polym. Phys. **40**, 2800–2806 (2002).
23. W. Watanabe, S. Sowa, T. Tamaki, K. Itoh, and J. Nishii, "Three-dimensional waveguides fabricated in poly(methyl methacrylate) by a femtosecond laser," Jpn. J. Appl. Phys. **45**, L765–L767 (2006).
24. A. Zoubir, C. Lopez, M. Richardson, and K. Richardson, "Femtosecond laser fabrication of tubular waveguides in poly (methyl methacrylate)," Opt. Lett. **29**, 1840–1842 (2004).
25. K. Wang, D. Klimov, and Z. Kolber, "Waveguide fabrication in PMMA using a modified cavity femtosecond oscillator," Proc. SPIE **6766**, 67660Q (2007).
26. K. Ohta, M. Kamata, M. Obara, and N. Sawanobori, "Optical waveguide fabrication in new glasses and PMMA with temporally tailored ultrashort laser," Proc. SPIE **5340**, 172 (2004).
27. C. R. Mendonca, L. R. Cerami, T. Shih, R. W. Tilghman, T. Baldacchini, and E. Mazur, "Femtosecond laser waveguide

micromachining of PMMA films with azoaromatic chromophores," Opt. Express **16**, 200–206 (2008).
28. G. Zhou, M. J. Ventura, M. R. Vanner, and M. Gu, "Use of ultrafast-laser-driven microexplosion for fabricating three-dimensional void-based diamond-lattice photonic crystals in a solid polymer material," Opt. Lett. **29**, 2240–2242 (2004).
29. M. Straub and M. Gu, "Near-infrared photonic crystals with higher-order bandgaps generated by two-photon photopolymerization," Opt. Lett. **27**, 1824–1826 (2002).
30. D. F. Farson, H. W. Choi, C. Lu, and L. J. Lee, "Femtosecond laser bulk micromachining of microfluidic channels in poly (methyl methacrylate)," J. Laser Appl. **18**, 210–215 (2006).
31. M. Haiducu, M. Rahbar, I. G. Foulds, R. W. Johnstone, D. Sameoto, and M. Parameswaran, "Deep-UV patterning of commercial grade PMMA for low-cost, large-scale microfluidics," J. Micromech. Microeng. **18**, 115029–115035 (2008).
32. Y. V. White, M. Parrish, X. Li, L. M. Davis, and W. Hofmeister, "Femtosecond micro- and nano-machining of materials for microfluidic applications," Proc. SPIE **7039**, 70390J (2008).
33. D. Gómez, I. Goenaga, I. Lizuain, and M. Ozaita, "Femtosecond laser ablation for microfluidics," Opt. Eng. **44**, 051105 (2005).
34. D. Day and M. Gu, "Microchannel fabrication in PMMA based on localized heating by nanojoule high repetition rate femtosecond pulses," Opt. Express **13**, 5939–5946 (2005).
35. S. Juodkazis, K. Yamasaki, A. Marcinkevicius, V. Mizeikis, S. Matsuo, H. Misawa, and T. Lippert, "Microstructuring of silica and polymethylmethacrylate glasses by femtosecond irradiation for MEMS applications," Mater. Res. Soc. Symp. Proc. **687**, B5.25 (2002).
36. E. G. Gamaly, A. V. Rode, V. T. Tikhonchuk, and B. Luther-Davies, "Ablation of solids by femtosecond lasers: ablation mechanism and ablation threshold for metals and dielectrics," Phys. Plasmas **9**, 949–957 (2002).
37. J. Kruger and W. Kautek, "Ultrashort pulse laser interaction with dielectrics and polymers," Adv. Polym. Sci. **168**, 247–289 (2004).
38. W. Watanabe, "Femtosecond filamentary modifications in bulk polymer materials," Laser Phys. **19**, 342–345 (2009).
39. H. Mochizuki, W. Watanabe, R. Ezoe, T. Tamaki, Y. Ozeki, K. Itoh, M. Kasuya, K. Matsuda, and S. Hirono, "Density characterization of femtosecond laser modification in polymers," Appl. Phys. Lett. **92**, 091120 (2008).
40. H. Mochizuki, W. Watanabe, Y. Ozeki, K. Itoh, K. Matsuda, and S. Hirono, "Fabrication of diffractive optical elements inside polymers by femtosecond laser irradiation," Thin Solid Films **518**, 714–718 (2009).
41. S. Baudach, J. Kruger, and W. Kautek, "Femtosecond laser processing of soft materials," Rev. Laser Eng. **29**, 705–709 (2001).
42. N. Bityurin, B. S. Luk'yanchuk, M. H. Hong, and T. C. Chong, "Models for laser ablation of polymers," Chem. Rev. **103**, 519–552 (2003).
43. M. Prasad, P. F. Conforti, and B. J. Garrison, "On the role of chemical reactions in initiating ultraviolet laser ablation in poly(methyl methacrylate)," J. Appl. Phys. **101**, 103113 (2007).
44. L. Torrisi, A. Lorusso, V. Nassisi, and A. Picciotto, "Characterization of laser ablation of polymethylmethacrylate at different laser wavelengths," Radiat. Eff. Defects Solids **163**, 179–187 (2008).
45. N. Bityurin, "Studies on laser ablation of polymers," Annu. Rep. Prog. Chem. Sect. C **101**, 216–247 (2005).
46. H. Huang and Z. Guo, "Ultra-short pulsed laser PDMS thin-layer separation and micro-fabrication," J. Micromech. Microeng. **19**, 055007 (2009).
47. A. Baum, P. J. Scully, W. Perrie, D. Liu, and V. Lucarini, "Mechanisms of femtosecond laser-induced refractive index modification of poly(methyl methacrylate)," J. Opt. Soc. Am. B **27**, 107–111 (2010).
48. C. G. Khan Malek, "Laser processing for bio-microfluidics applications (part I)," Anal. Bioanal. Chem. **385**, 1351–1361 (2006).
49. C. G. Khan Malek, "Laser processing for bio-microfluidics applications (part II)," Anal. Bioanal. Chem. **385**, 1362–1369 (2006).
50. C. Monat, P. Domachuk, and B. J. Eggleton, "Integrated optofluidics: a new river of light," Nat. Photonics **1**, 106–114 (2007).
51. J. H. Si, J. R. Qiu, J. F. Zhai, Y. Q. Shen, and K. Hirao, "Photoinduced permanent gratings inside bulk azodye-doped polymers by the coherent field of a femtosecond laser," Appl. Phys. Lett. **80**, 359–361 (2002).
52. L. Ding, D. Jani, J. Linhardt, J. F. Künzler, S. Pawar, G. Labenski, T. Smith, and W. H. Knox, "Large enhancement of femtosecond laser micromachining speed in dye-doped hydrogel polymers," Opt. Express **16**, 21914–21921 (2008).
53. L. Ding, R. I. Blackwell, J. F. Kunzler, and W. H. Knox, "Femtosecond laser micromachining of waveguides in silicone-based hydrogel polymers," Appl. Opt. **47**, 3100–3108 (2008).
54. J. Si, Z. Meng, S. Kanehira, J. Qiu, B. Hua, and K. Hirao, "Multiphoton-induced periodic microstructures inside bulk azodye-doped polymers by multibeam laser interference," Chem. Phys. Lett. **399**, 276–279 (2004).
55. J. H. Si, J. R. Qiu, J. F. Zhai, Y. Q. Shen, and K. Hirao, "Photoinduced permanent gratings inside bulk azodye-doped polymers by the coherent field of a femtosecond laser," Appl. Phys. Lett. **80**, 359–361 (2002).
56. T. N. Kim, K. Campbell, A. Groisman, D. Kleinfeld, and C. B. Schaffer, "Femtosecond laser-drilled capillary integrated into a microfluidic device," Appl. Phys. Lett. **86**, 201106 (2005).
57. S. Demming, A. Llobera, R. Wilke, and S. Büttgenbach, "Single and multiple internal reflection poly(dimethylsiloxane) absorbance-based biosensors," Sens. Actuators B: Chem. **139**, 166–173 (2009).
58. S. K. Sia and G. M. Whitesides, "Microfluidic devices fabricated in poly(dimethylsiloxane) for biological studies," Electrophoresis **24**, 3563–3576 (2003).
59. J. C. McDonald, D. C. Duffy, J. R. Anderson, D. T. Chiu, H. Wu, O. J. A. Schueller, and G. M. Whitesides, "Fabrication of microfluidic systems in poly(dimethylsiloxane)," Electrophoresis **21**, 27–40 (2000).
60. A. C. Siegel, D. A. Bruzewicz, W. B. Weibel, and G. M. Whitesides, "Microsolidics: fabrication of three-dimensional metallic microstructures in poly(dimethylsiloxane)," Adv. Mater. **19**, 727–733 (2007).
61. T. O. Yoon, H. J. Shin, S. C. Jeoung, and Y-II. Park, "Formation of superhydrophobic poly(dimethylsiloxane) by ultrafast laser-induced surface modification," Opt. Express **16**, 12715–12725 (2008).
62. D. B. Wolfe, J. B. Ashcom, J. C. Hwang, C. B. Schaffer, E. Mazur, and G. M. Whitesides, "Customization of poly (dimethylsiloxane) stamps by micromachining using a femtosecond-pulsed laser," Adv. Mater. **15**, 62–65 (2003).
63. S. Chung, J. H. Lee, M.-W. Moon, J. Han, and R. D. Kamm, "Non-lithographic wrinkle nanochannels for protein preconcentration," Adv. Mater. **20**, 3011–3016 (2008).
64. S.-H. Cho, W.-S. Chang, K.-R. Kim, and J. W. Hong, "Femtosecond laser embedded grating micromachining of flexible PDMS plates," Opt. Commun. **282**, 1317–1321 (2009).
65. K. C. Vishnubhatla, S. Venugopal Rao, R. S. S. Kumar, M. Ferrari, and D. Narayana Rao, "Optical characterization of micro-structures in silicate, FOTURAN™ and tellurite glasses inscribed by femtosecond laser direct writing," Opt. Commun. **282**, 4537–4542 (2009).
66. K. C. Vishnubhatla, S. Venugopal Rao, R. S. S. Kumar, R. Osellame, S. N. B. Bhaktha, S. Turrell, A. Chiappini, A. Chiasera, M. Ferrari, M. Mattarelli, M. Montagna, R. Rampo-

ni, G. C. Righinini, and D. Narayana Rao, "Direct writing of waveguides and gratings in 'BACCARAT' glass using femtosecond pulses," J. Phys. D **42**, 205106 (2009).
67. C. B. Schaffer, A. Brodeur, and E. Mazur, "Laser-induced breakdown and damage in bulk transparent materials induced by tightly focused femtosecond laser pulses," Meas. Sci. Technol. **12**, 1784–1794 (2001).
68. A. Carrington and G. Stein, "Free radical formation and oxygen effect in irradiated polymethylmethacrylate," Nature **193**, 976 (1962).
69. H. Y. Kaptan and O. Guven, "Effect of γ-irradiation dose for the oxygen diffusion into polymers," J. Appl. Polym. Sci. **64**, 1291–1294 (1997).
70. H. Y. Kaptan and L. Tatar, "An electron spin resonance study of mechanical fracture of poly(methyl methacrylate)," J. Appl. Polym. Sci. **65**, 1161–1167 (1997).
71. F. Szocs, "Free radicals in x-ray irradiated poly (methylmethacrylate) from the point of view of ESR dosimetry," Chem. Papers **53**, 137–139 (1999).
72. M. Velter-Stefanescu, O. G. Duliua, and N. Preda, "On the relaxation mechanisms of some radiation induced free radicals in polymers," J. Optoelectron. Advanced Mater. **7**, 985–989 (2005).
73. R. E. Samad, L. C. Courrol, A. B. Lugão, A. Z. de Freitas, and N. D. V. Junior, "Production of color centers in PMMA by ultrashort laser pulses," Radiat. Phys. Chem. **79**, 355–357 (2010).